Separating Volcanic Deformation and Atmospheric Signals at Mount St. Helens Using Persistent Scatterer InSAR

Corresponding Author
Mark D Welch[a] - mdw12@uw.edu

David A Schmidt[a] - dasc@uw.edu

[a] University of Washington, Department of Earth and Space Sciences
Postal Address: University of Washington, Johnson Hall Rm-070, Box 351310, 4000 15th Avenue NE, Seattle, WA 98195-1310

Abstract

Over the past two decades, GPS and leveling surveys have recorded cycles of inflation and deflation associated with dome building eruptions at Mount St. Helens. Due to spatial and temporal limitations of the data, it remains unknown whether any deformation occurred prior to the eruption of 2004. Interferometric Synthetic Aperture Radar (InSAR), with its fine spatial resolution, has the potential to resolve pre-eruptive deformation that may have occurred, but eluded detection by campaign GPS surveys because it was localized to the edifice or crater. Traditional InSAR methods are challenging to apply in the Cascades volcanic arc because of a combination of environmental factors. Past attempts to observe deformation at Mount St. Helens were unable to make reliable observations in the crater or on much of the edifice.

In this study, Persistent Scatterer InSAR, known to mitigate issues of decorrelation caused by environmental factors, is applied to four SAR data sets in an attempt to resolve localized sources of deformation on the mountain from 1995-2010. Many interferograms are strongly influenced by phase delay from atmospheric water vapor, and must be corrected. To assess the bias imposed by the atmosphere, we perform sensitivity tests on a suite of atmospheric correction techniques, including several that rely on the correlation of phase delay to topography. We also explore approaches that directly estimate phase delay using the ERA-Interim climate reanalysis data set. We find that phase-based corrections and the ERA-Interim atmospheric correction produce velocities on the edifice of Mount St. Helens that differ by up to 1 cm/yr due to variability in how atmospheric artifacts are treated in individual interferograms. Additionally, simple phase-based techniques run the risk of minimizing any surface deformation signals. The PS InSAR results for overlapping tracks are inconsistent with one another, and do not provide conclusive evidence for any pre-eruptive deformation at a broad scale or localized to the crater or edifice leading up to the 2004 eruption. However, we cannot rule out the possibility of deformation less than ~5 mm/yr, or discern whether deformation rates increased in the preceding months. The results do, however, significantly improve the spatial density of

observations and also our ability to resolve or rule out models for a potential deformation source for the pre-eruptive period.

1. Introduction and Motivation

Since its explosive eruption in 1980, Mount St. Helens has undergone cyclic inflation and deflation associated with dome building eruptions and the re-pressurization of its magmatic system at depth (Palano et al., 2012). The record of surface deformation at Mount St. Helens over that time period is incomplete, and what is known was measured primarily by ground based geodetic techniques including GPS and trilateration surveys (Lisowski et al., 2008; Dzurisin et al., 2008). Prior to the dome building eruption 2004, that began on October 1, surveys of deformation were both temporally and spatially coarse. Campaign GPS and trilateration surveys were conducted with repeat intervals of one to three years, and the closest continuous GPS station was located 9km from the crater at the Johnston Ridge Observatory (Dzurisin, 2003). The results of these surveys revealed that following the eruption of 1980, a broad region surrounding the edifice underwent surface dilatation, indicating expansion and presumably the recharge of a deep magma reservoir (Lisowski et al., 2008). Interestingly, this expansion ceased some time before 1991, and deformation on that scale was not detected again until two weeks before the 2004 eruption, coincident with the onset of seismic unrest (Dzurisin et al., 2008). Because none of these surveys were capable of making accurate measurements on the edifice itself, it is possible that pre-eruptive deformation did occur, but was localized to the edifice or crater.

The eruption in 2004 spurred the installation of additional continuous GPS stations in the proximity of Mount St. Helens (Dzurisin et al., 2008). This updated network was able to record the co-eruptive deflation and the transition back to a phase of inflation, which continues through 2016 (Palano et al., 2012). As in the past, the subtle surface deformation signal at St Helens continues to be monitored primarily by ground based geodetic techniques.

The remote sensing tool Interferometric Synthetic Aperture Radar (InSAR) has the potential to substantially augment these techniques by providing spatially dense, precise measurements of surface displacements, and may also reveal other volcanic or surficial processes too localized to be detected by ground based methods. InSAR methods are capable of producing time-series of deformation with millimeter precision at a resolution of meters to tens-of-meters over study areas ranging from kilometers to hundreds-of-kilometers in extent (Zebker et al., 2000; Simons and Rosen, 2007).

Traditional SAR interferometry is challenging to apply to the stratovolcanoes of the Cascades, but has been implemented successfully in the past, observing deformation at Medicine Lake and Three Sisters Volcanoes (Wicks et al. 2002; Poland et al., 2006; Poland and Lu, 2008; Dzurisin et al., 2009; Riddick and Schmidt, 2011). Widespread phase decorrelation caused by persistent snow cover and dense vegetation, combined with large orographic elevation dependent atmospheric phase delays, mask or make deformation signals difficult to detect. The combination of these factors impeded previous attempts to image pre-eruptive deformation at Mount St. Helens using standard interferometry and stacking (Poland and Lu, 2008). These authors were able to image the co-eruptive deflation signal that was also observed by the newly installed GPS instruments, but the results from InSAR for the time period preceding the 2004 eruption were inconclusive with respect to volcanic deformation.

By applying the StaMPS (Stanford Method for Persistent Scatterers) Persistent Scatterers (PS) technique, phase decorrelation in challenging study areas, like Mount St. Helens, can be mitigated by utilizing only the pixels with the highest, statistically derived, signal-to-noise ratio in a time-series composed of many interferograms (Hooper et al., 2012). The persistent scatterer technique has been shown to vastly improve the coherence and number of reliable observations in natural terrains around the world, exemplified by a study of Volcan Alcedo in the Galapagos and a study of slow-slip in Guerrero, Mexico (Hooper et al., 2007; Hooper et al., 2012).

Even if a coherent signal can be obtained on the edifice of Mount St. Helens using the PS technique, additional work must be done to separate potential deformation from atmospheric phase delay, the largest remaining source of error for current InSAR studies (Hannsen, 1998). Atmospheric phase delay arises primarily in interferometry when the distribution of water vapor present in the troposphere differs between the two SAR scenes. Changes in water vapor content alter the refractivity of the atmosphere, which leads to a phase delay in the interferograms (Zebker et al., 1997). Atmospheric phase delay is often correlated with surface topography, and under certain circumstances, appears as a radially symmetric surface deformation signal centered over a volcano (Beauducel et al., 2000). The phase signal associated with changes in atmospheric refractivity is often broken down into a stratified and a turbulent component (Hanssen, 2001). The stratified component is elevation dependent and spatially correlated over large distances, while the turbulent component is related to small scale or stochastic atmospheric variations and cannot be modeled simply.

There are a variety of techniques available for estimating and removing the stratified component of atmospheric delay, which fall into two major groups. The first group of methods relies on the relationship between phase delay and the elevation of a given point (Beauducel et al., 2000; Remy et al., 2003; Ding et al., 2008). A linear or power-law function can be fit to the phase and elevation data to estimate and remove the atmospheric signal. However, because volcanic deformation is also often strongly correlated with elevation, it is extremely difficult to distinguish between the two with a single or small number of interferograms, and attempts to model the atmospheric noise at volcanoes with this technique run the risk of removing the desired deformation signal along with the atmospheric noise.

The second category of atmospheric removal techniques uses an independent data set to estimate or model the atmospheric phase delay (Foster et al., 2013; Jolivet et al., 2014, Bekaert et al., 2015b). These data sets typically provide measurements of pressure, temperature, and water vapor as a function of altitude. The vertical profiles are derived either

from measurements made by satellite borne instruments including NASA's MODIS and MERIS, or from climate reanalysis models such as ERA-Interim, WRF, and NARR. Measurements made by instruments like MODIS and MERIS are not always ideal, as the data typically have low spatial resolution, especially at night, and are only usable in the absence of clouds. The MERIS instrument, which was mounted on the European Space Agency's Environmental Satellite (ENVISAT) is particularly useful for correcting phase delay in interferograms generated with SAR data from that mission, as the atmospheric and radar data are collected concurrently. Corrections made with climate reanalysis models benefit from the fact that they incorporate multiple data sources and techniques used for weather prediction to improve temporal resolution to 4-8 time-steps per day. However, this may still be insufficient to capture some transient atmospheric events.

Maps of predicted phase delay are generated by spatially interpolating measured vertical profiles of pressure, temperature, and water vapor to cover the SAR scene at the desired resolution. These profiles can be transformed into profiles of refractivity (equation 1) which are then used to calculate the integrated phase delay along the line of sight path for a given pixel in an interferogram using equation 2 (Hanssen, 2001; Bekaert et al., 2015a). Refractivity (N), is a combination of total atmospheric pressure (P), temperature (T), partial pressure of water vapor (e), and empirical constants (k_1, k'_2, and k_3). Tropospheric phase delay (ϕ_{tropo}) is the integral of refractivity from the elevation of the ground surface (h1) to the top of the troposphere (h_{top}), multiplied by geometric factors dependent on the radar incidence angle (θ) and the radar wavelength (λ).

Equation 1. $N=(k_1*P/T)_{hydr} + (k_2'*e/T + k_3*e/T^2)_{wet}$

Equation 2. $\phi_{tropo} = (-4*\pi/\lambda)*(10^{-6}) / \cos(\theta) * \int_{h=h1}^{h=h_{top}} N(h)dh$

In this study, we attempt to resolve the near-field deformation on Mount St. Helens using PS InSAR. SAR data from the ERS-2 and ENVISAT missions spanning more than fifteen years (1995-2010) are processed with the StaMPS package to image the surface deformation associated with a complete eruptive cycle of Mount St. Helens. The low signal-to-noise ratio prompts us to carefully consider potential biases, particularly from atmospheric water vapor delay. In order to confidently interpret anomalies in the signal as volcanic deformation, the effect of atmospheric phase delay must be minimized and the biases associated with the analysis and correction techniques well understood. A series of sensitivity tests are conducted to assess the bias imposed by both the atmospheric phase delay and the choice of method used to correct it. The removal techniques tested in this study include a variety of approaches for fitting trends in phase and elevation and also models of phase derived from ERA-Interim climate reanalysis data. Each atmospheric correction is applied to the data within the StaMPS framework to deduce its effect on PS velocities and the time series of deformation.

2. SAR and Atmospheric Data Description

Four separate SAR data sets were processed using the persistent scatterer processing package StaMPS in order to image any pre-eruptive or post-eruptive deformation associated with the 2004 eruption of Mount St. Helens. Two tracks from the European Space Agency's ERS-2 satellite cover the pre-eruptive period, while two from their ENVISAT mission cover the post-eruptive period. The number and size of available and appropriate data sets, listed in Table 1, are limited by the 35-day repeat interval and prioritization of targets to be imaged by the satellite, and also by a variety of factors relating to the coherence or quality of interferograms. For much of the year, the edifice of Mount St. Helens is covered in deep snow. To minimize the effect of snow and maximize the area of coherent phase, only SAR acquisitions from the

summer and fall months (June-October) were considered.

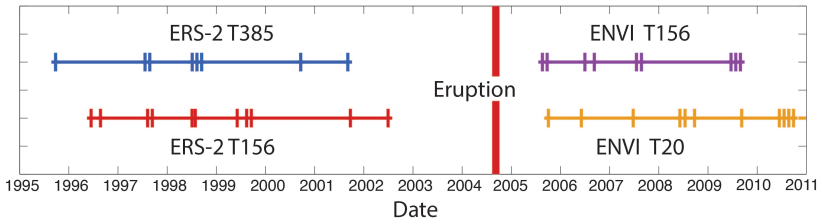

Figure 1. Timeline of SAR scenes for four data sets covering the pre- and post-eruptive periods. The vertical red bar indicates the onset of the 2004 eruption on October 1st.

Satellite	Scenes	Track	Frame	Master	Start	End
ERS-2	8	385	2673	8/28/98	9/24/95	9/2/01
ERS-2	11	156	2673	8/9/98	6/14/96	6/28/02
ENVISAT	11	156	2673	6/6/08	8/17/05	8/26/09
ENVISAT	9	20	909	7/18/07	9/30/05	9/24/10

Table 1. A summary of SAR data used in this study.

Under the standard StaMPS processing routine, all interferograms share a common master scene. The master scene for each data set (Table 1) is chosen by minimizing the sum decorrelation from the temporal and perpendicular baselines of the SAR scenes using the technique outlined by Hooper et al. (2007), holding the Doppler centroid and thermal noise terms constant. When either the temporal or perpendicular baseline between the chosen master and a given scene is too large, the resulting interferogram will be incoherent and so the scene is excluded from the data set. To maximize the signal-to-noise for surface velocities, only data sets with more than eight scenes were processed in this study. The ground surface in the area surrounding Mount St. Helens, especially within the crater, was modified during the 2004 eruption, repositioning the scattering elements on the ground. This leads to significant decorrelation. Thus, interferograms spanning the eruption were not made or utilized in the time series analysis.

NASA's SRTM digital elevation model (DEM) was used to remove the topographic phase from interferograms with dates prior to 2004 (Farr and Kobrick, 2000). Interferograms for the post-eruptive period were corrected using a hybrid of SRTM and LiDAR (Mosbrucker, 2014) DEM's in order to accurately represent the major changes to topography by spine emplacement and dome building within the crater of Mount St. Helens (Scott et al., 2008). The hybrid elevation model was constructed by creating a mosaic of the two data sets in ArcMAP, giving priority to the LiDAR data set. A weighted average of the SRTM and LiDAR data was then conducted for pixels near the edges of the smaller LiDAR data set to reduce jumps at the boundaries.

The atmospheric phase delay corrections were made using the ERA-Interim global atmospheric reanalysis data set produced by the European Centre for Medium-Range Weather Forecasts (ECWMF). Estimates of past atmospheric conditions are made by integrating a range of observations into coupled models of the climate system (Dee et al., 2011). The model produces vertical profiles of pressure, humidity, and temperature with data-points at 60 pressure levels from the earth's surface to an altitude corresponding to 0.1 hPa. The vertical profiles are generated at six-hour spacing and a horizontal resolution of 80 km. Because the time steps of the ERA-Interim model differ from the timing of radar acquisitions, the atmospheric data must be interpolated temporally, which can potentially introduce significant error, especially in cases of rapidly changing weather conditions.

3. Methods

3.1 InSAR data processing

Four SAR data sets, spanning the time period from September 1995-2010, were processed with the Persistent Scatterer software package (StaMPS / MTI) developed by Hooper and others (2012). The StaMPS methodology requires that a single scene be chosen as the

master image for all of the interferograms in a data set. In each case, the perpendicular and temporal baselines were calculated for all possible interferogram pairs and a master was selected by minimizing the combined expected effect of the spatial and temporal baselines. Multiple master scene candidates with low expected decorrelation were tested for each data set and the master which produced the most visually coherent interferograms was selected. After a master was chosen, interferograms were generated using the basic routine outlined in the StaMPS / MTI software package. To reduce the required computing power and processing time, the SAR scenes were cropped to an area centered over Mount St. Helens with dimensions on the order of 20km-by-40km. Interferograms were visually inspected for quality and those with no distinguishable visible coherence were discarded. The remaining set of geo-coded interferograms were imported into the MATLAB based StaMPS framework, where stable PS pixels are selected, and average velocities and time-series calculated.

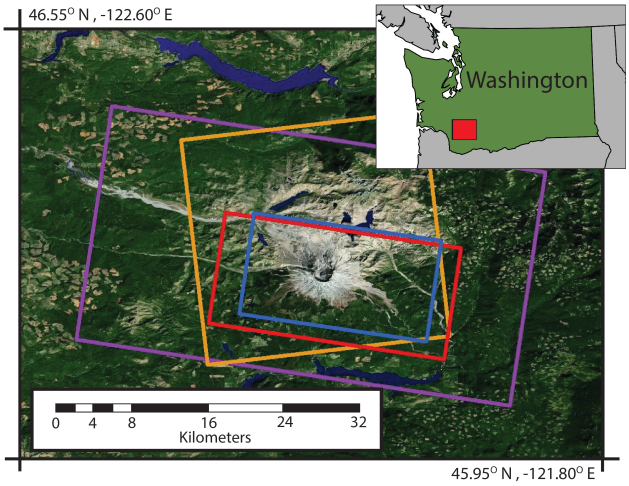

Figure 2. Location and coverage of cropped SAR scenes for the four data sets. ERS-2 tracks 385 and 156 are in blue and red, respectively, while ENVISAT tracks 156 and 20 are in purple and yellow, respectively. Location relative to the state of Washington is shown in the inset map.

3.2 StaMPS methodology

The StaMPS method can significantly reduce the effects of decorrelation and improve signal-to-noise in interferometric results by statistically identifying pixels with the least stochastic noise and using only those pixels in the final products. To estimate the random noise of a pixel, the contribution to the interferometric phase from deformation, atmosphere, orbit error, and DEM error is estimated and removed. The phase contribution from each of these sources is estimated using a combination of spatial and temporal filters, and also correlative relationships between phase and perpendicular baseline. By removing these deterministic contributors to phase from the time-series of each pixel, an estimate for the stochastic component of the noise through time is obtained. Pixels whose resulting time-series of stochastic noise have the least variance, or in other words, are the least noisy and most stable through time, are selected as PS pixels (Hooper et al., 2007; 2012). Using the more reliable PS pixel candidates, the models of the deterministic contributors to phase can be refined. This process is repeated until it converges on a statistically robust set of pixels with high signal-to-noise, such that less than five percent of the pixels are false positive stable scatterers. While we expect the selected PS pixels to have a very low amount of random noise, it can still be extremely difficult to distinguish between, and separately quantify, the phase contributions of the deterministic factors. The phase delay introduced by the atmosphere can be especially difficult to differentiate from the desired deformation signal because of its large amplitude, and nearly identical spatial characteristics. Often, both the atmospheric and volcanic deformation signals have spatial wavelengths on the order of several kilometers, and are centered over the edifice. This issue can be overcome to a degree by increasing the number of scenes in the SAR data set, leveraging the fact that atmospheric delay is uncorrelated over timescales longer than one day (Emardson et al., 2003).

Parker and others (2015) demonstrated that in the Cascade volcanic arc, between 4 and 11 consecutive interferograms are required to average out the atmospheric variability enough to

detect a volcanic deformation signal with an average velocity of 1 cm/yr. The authors predict that a minimum of 6-8 interferograms would be needed in the case Mount St. Helens, which indicates that the size of the data sets in this study should be sufficient for detecting a 1 cm/yr signal, but that they may be near the limit. In order to increase precision and the chances of detecting a subtle signal, techniques for correcting atmospheric phase delay must be applied.

3.3 Atmospheric Testing

Many approaches for modeling and removing atmospheric phase delay from interferograms exist and can be simply implemented within the framework of the StaMPS software. A sensitivity test was conducted to assess the impact of the choice of atmospheric removal technique on the surface velocities obtained with PS methods. This was accomplished by applying a suite of different correction techniques to the larger of the two ERS-2 data sets. A variety of approaches towards modeling phase delay using the phase-elevation correlation were tested along with the ERA-Interim climate reanalysis derived model.

The models that utilize the correlation between tropospheric phase delay ($\Delta\phi_{tropo}$) and elevation (h) assumed three basic forms, either a linear, power-law, or windowed moving average relationship between the two variables. In the case of the power-law fit, the form of the equation is as follows (from Bekaert et al., 2015a):

$$\text{Equation 1.} \qquad \Delta\phi_{tropo} = K' (h_0 - h)^a$$

In this form, K' is the coefficient which relates phase to elevation, h_0 (assumed to be 7000m) is the reference height above which the atmosphere is considered stable, and 'a' is the power-law exponent, often determined from balloon sounding data, assumed to have a value of 1.6 in this study. The window size used for the moving average was 300m of elevation. Modified versions of the linear and power-law fit models were also tested. In the modified models, the free parameters relating phase and elevation data were calculated using only specific spatial

subsets of the PS pixels. The advantage of spatial subsampling is that some data points are likely more representative of the physical correlation between phase delay and elevation specifically over the edifice of Mount St. Helens. The subsets tested were defined as: all points within 4km of the crater center, all points above an elevation of 1300 meters, all points excluding suspected pumice plain deformation, and a set of points down-sampled 10x with an even distribution over the range of elevations. One additional modification of the trend fitting process that was tested was to weight each pixel in the inversion by a metric of its phase stability, determined by StaMPS, so that noisier pixels have less effect on the fit. This weighting scheme was applied to all other phase-elevation fitting corrections to compare weighted and un-weighted results.

Models of atmospheric phase delay that incorporate data from the ERA-Interim climate reanalysis were generated using the freely available Toolbox for Reducing Atmospheric InSAR Noise (TRAIN) developed by David Bekaert et al. (2015b) and are seamlessly integrated into the StaMPS framework. The estimates of phase delay produced by TRAIN are derived from spatially and temporally interpolated vertical profiles of measured and modeled meteorological parameters. Phase delay for each PS pixel is calculated as the integral of refractivity along the line of sight from the satellite to the ground (Hannsen, 2001; Bekaert et al., 2015).

3.4 Statistical Analysis and Synthetic Modeling

Each atmospheric correction method produces a map of phase delay for all interferograms in the data set, which are then integrated into StaMPS to produce 23 line of sight velocity and time series products. The standard deviation of velocities for each pixel was calculated to demonstrate the possible magnitude of bias inherent in the choice of an atmosphere correction method. Next, a jack-knife analysis (i.e. Agram and Simons, 2015) was applied to the 23 average velocity data sets by individually removing each set and recalculating

the mean and standard deviation of velocities. This test determines which corrections had the largest effect on the variance, or differed the most from the mean.

To assess whether phase-elevation based modeling techniques might potentially remove any desired volcanic deformation signal at Mount St. Helens, a synthetic test was carried out. First, a set of common-master, synthetic interferograms containing deformation signal from a spheroidal magma chamber, expanding at a constant rate were generated using the dMODELS written by Battaglia et al. (2013). The depth to the chamber and pressure increase were set to be 2000 meters and 1250 MPa respectively, to create a substantial velocity signal of 15mm/yr. Next, the ERA-Interim derived correction was added into each interferogram to simulate atmospheric noise and then modeled and removed using a linear fit to phase and elevation within the StaMPS framework. The resulting maximum velocities over the edifice were compared to the expectations based on the spheroidal model to quantify the error or bias introduced by using the linear phase based technique.

4. Results

4.1 Individual Interferograms

The individual interferograms processed in this work all have significant areas of decorrelation caused by the factors discussed earlier. With the exception of two interferograms, created with slave scenes acquired within two months of the master, coherence was limited to areas lacking both dense vegetation and persistent snow cover, namely recent lava flows, the pumice plain, and lower edifice. The map in Figure 3 shows the distribution of dense forest, surface water, and ice, where low coherence is expected. The effect of atmospheric phase delay is clearly visible in the coherent regions of many interferograms with one, or in some cases two, phase cycles correlated with elevation on the edifice, corresponding to 2.8 to 5.6 cm of apparent surface deformation. Also visible in several interferograms is a signal of subsidence occurring on the pumice plain to the northwest of Mount St. Helens.

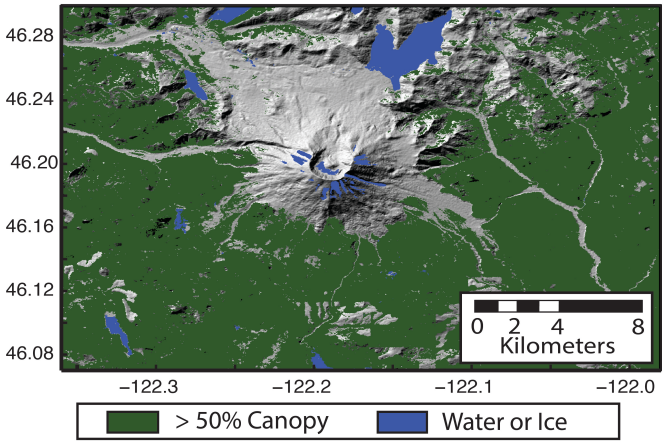

Figure 3. Environmental factors known to negatively affect interferometric coherence are shown in color, overlaid on a hill-shaded digital elevation model. Green indicates areas with greater than 50% canopy cover while blue indicates either surface water or ice (NLCD). Coherence in interferograms correlates very well with the absence of the environmental factors (see Figure 4).

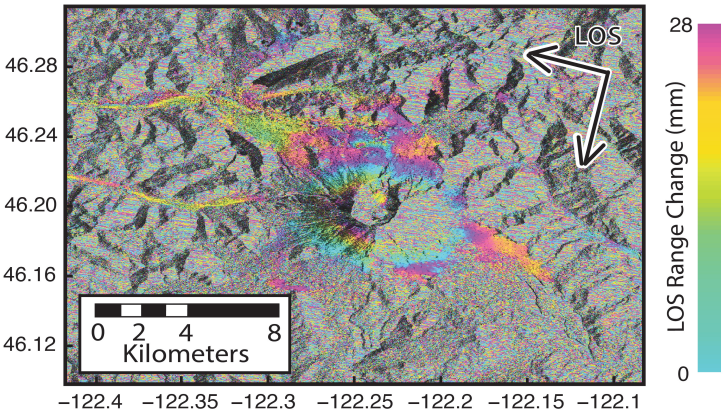

Figure 4. Example geocoded interferogram from the descending ERS-2 track 156 data set spanning 9/12/1997 – 8/28/1998, overlain on radar amplitude image. One cycle (fringe) of color indicates 28mm of displacement. Fringes indicating atmospheric phase delay correlated to topography on the edifice can be seen clearly, summing to an apparent displacement of ~30mm. A subsidence signal on the pumice plain north of the crater is also visible.

4.2 Persistent Scatterer Velocities

The StaMPS algorithm identifies on the order of 10,000 persistent scatterer pixels in each SAR scene, whose locations correlate very well with regions of high spatial coherence in interferograms and with mapped regions of low vegetation, snow, or ice cover. PS pixels are

identified on all parts of the Mount St. Helens' edifice and within the crater, but in far lower densities than on the pumice plain and lower slopes of the mountain.

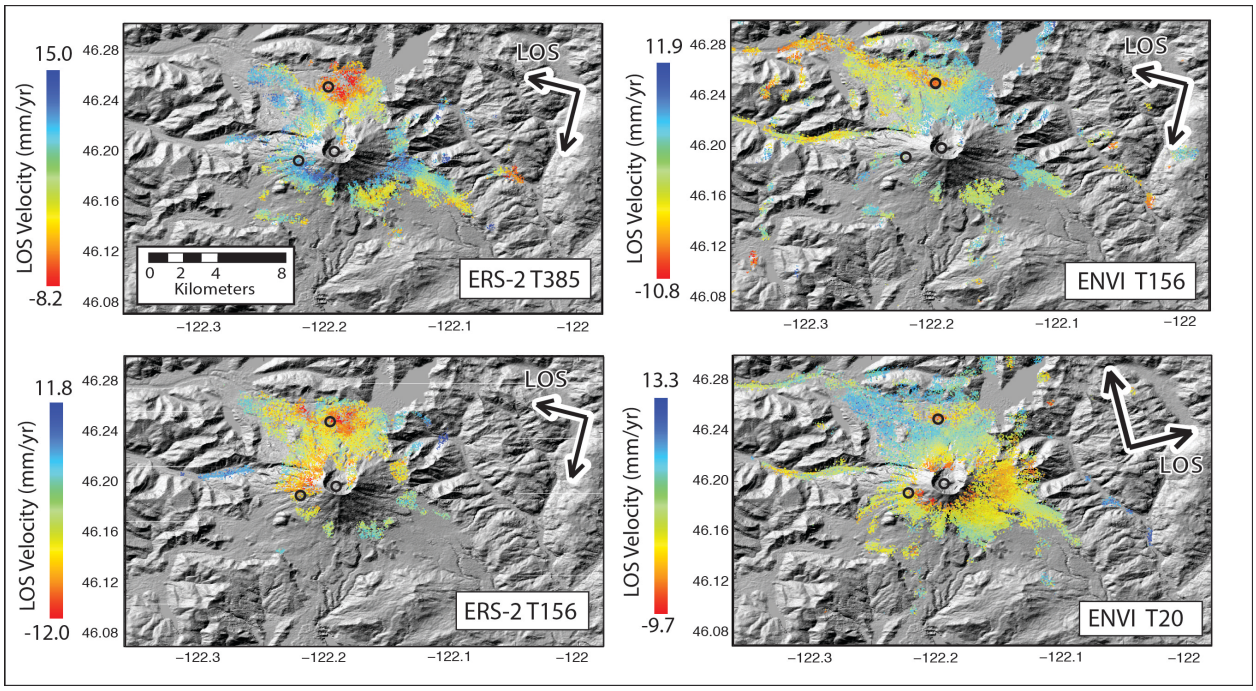

Figure 5. PS average velocities for the four data sets lain over a shaded relief DEM. Pre-eruptive data sets are on the left and post-eruptive on the right. Areas with less than 50 pixels/km^2 are masked out to highlight areas where phase-unwrapping errors are unlikely. Open black circles indicate the locations of time series plotted in Figure 6. Arrows in upper right of each map indicate the radar line of sight (LOS) and satellite flight direction (perpendicular).

PS InSAR results for the crater and edifice during the pre- and post-eruptive period reveal LOS (Line of Sight) velocities less than 1 cm/yr (Figure 5) suggesting that any signal is at or below the level of the noise. In addition, the apparent signal in those regions has opposite sign depending on the data set over the same time period. In the pre-eruptive period, ERS-2 track 385 indicates uplift of the edifice at a rate of approximately 5 mm/yr, while track 156 shows subsidence at a similar rate. For the post-eruptive period, ENVISAT track 156 indicates uplift of the edifice at a rate of approximately 10 mm/yr, while track 20 shows subsidence at roughly 8 mm/yr.

The subsidence signal on the pumice plain, first detected by Poland and Lu (2008), is seen clearly in all plots of average velocity for all data sets, regardless of atmospheric correction technique. The subsidence rate varies spatially and between data sets with a maximum detected rate of 10 mm/yr. By comparing pre- and post-eruptive velocity maps, the subsidence signal appears to migrate to the northwest and become more localized through time.

4.3 Time Series

Ground displacement time-series show in greater detail, the same findings as the average velocity plots. Time series for locations on the edifice and in the crater from all four data sets show that average velocities are low, and when comparing between data sets for the same time period, the displacement trends have opposite sense of direction (Figure 6). The time series for the two locations on the pumice plain show much more consistency between data sets, and suggest that the subsiding region migrated spatially through time. It can be seen that the time series for pixels on the edifice and crater have a good deal of scatter compared to their velocities (Figure 6). The discrepancies in velocities and time series for the edifice and crater become worse when atmosphere is not modeled and removed, indicating atmospheric modeling does improve the quality of the result. The application of the ERA-Interim correction method leads to an average reduction in the variance of time series for all pixels of 21.4 mm or 74 percent.

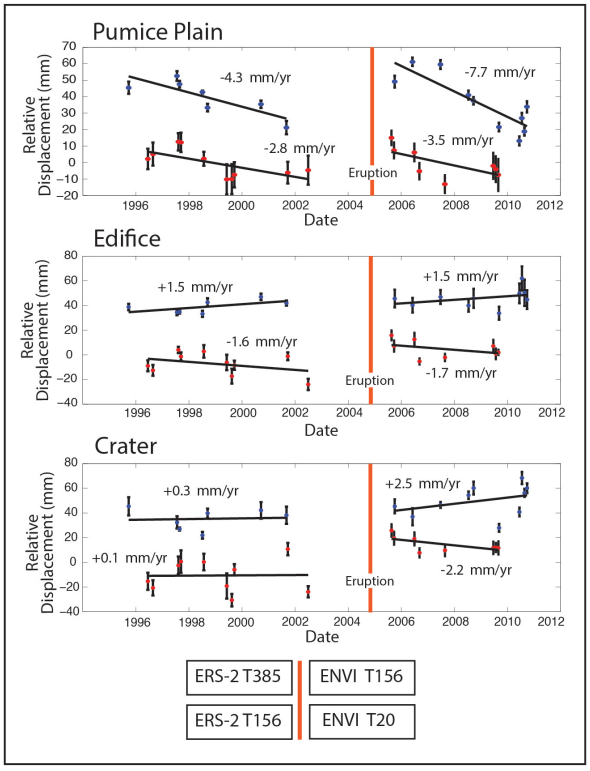

Figure 6. Time series of displacement and average velocities for three locations at Mount St. Helens across all four data sets. Each time-series shown is the average time-series for the set of all PS pixels within a circle of radius 200m, where the error-bars for each point represent one standard deviation for the set of displacements. Average velocity as the slope of the line of best fit is shown for each set. Displacements in InSAR are relative, not absolute, and so the time-series are shifted along the Y-axis for visual clarity. Map locations of the time-series are indicated as open black circles in Figure 5. The vertical red bar indicates the onset of the eruption. Pumice plain velocities indicate subsidence across all data sets, while the time-series for the crater and edifice do not show consistent deformation.

4.4 Sensitivity Test of Atmospheric Correction

Statistical and visual comparisons show that the vast majority of atmospheric correction techniques produce very similar LOS velocity results. In particular, results that utilize any modification of either a linear or power-law fit to the phase versus elevation data are virtually identical. This is shown clearly by the results of the jack-knife analysis (Table 2). When the velocities corrected by linear or power-law based models are removed from the set, the jack-knife mean does not change significantly from the mean of the full set. Furthermore, when

comparing a typical pair of phase based corrections, the average difference in velocity for a given pixel is only 0.13 mm/yr. or about 8.1%. For example, a linear fit restricted to points with elevations above 1300 meters, compared to using all of the PS points, results in a change in velocity of only 0.2 to 0.25 mm/yr for pixels on the edifice and less than 0.15 mm/yr for those in the majority of the surrounding region.

Correction Name	Average Change in Mean by Removal (mm/yr)	Average Standard Deviation after Removal (mm/yr)
ERA-Interim	0.036	0.16
Moving Average	0.014	0.23
Weighted Moving Average	0.012	0.23
Power-law Deformation Mask	0.009	0.24
Weighted Power-law Deformation Mask	0.009	0.24
Linear Deformation Mask	0.009	0.24
Weighted Linear Deformation Mask	0.009	0.24
Weighted Linear Distance Crop	0.007	0.24
Weighted Power-law Distance Crop	0.007	0.24
Linear Distance Crop	0.006	0.24
Power-law Distance Crop	0.006	0.24
Weighted Power-law No Crop	0.005	0.24
Weighted Linear No Crop	0.004	0.24
Power-law No Crop	0.004	0.24
Linear No Crop	0.004	0.24
Weighted Power-law Height Crop	0.003	0.24
Power-law Height Crop	0.003	0.24
Weighted Linear Height Crop	0.002	0.24
Linear Height Crop	0.002	0.24
Linear Downsampled	0.002	0.24
Power-law Downsampled	0.002	0.24
Weighted Linear Downsampled	0.002	0.24
Weighted Power-law Downsampled	0.002	0.24

Table 2. Jack-knife results show for the average pixel in the ERS-2 Track 156 data set, how different or similar the velocity produced by one particular atmospheric correction is to that of the full set of 23 different corrections. If for the average pixel, the mean velocity of the set changes greatly or the standard deviation of velocities is reduced by the removal of a correction, then it is dissimilar to the set. Apart from the ERA-Interim and moving average corrections, the choice of correction technique has little impact on the velocity results.

Models that utilize a moving average with an elevation window of 300m to predict atmospheric delay from phase produce results that are appreciably different from the other phase based techniques. When the moving average corrected velocities are removed from the

set, the standard deviation of velocities for the average pixel decreases by 4.3%, indicating its dissimilarity from other phase-based corrections. To further illustrate this point, the velocities predicted by the moving average correction are up to 2 mm/yr higher on the edifice than those from a linear model.

The jack-knife results in Table 2 also show that the ERA-Interim correction produces velocities that differ the most from the mean of all atmospheric corrections tested. Removal of the ERA-Interim correction reduces the standard deviation of velocities for the average pixel by 34%. Applying the ERA-Interim correction leads to velocities on the edifice and within the crater that have opposite sign to those from linear and power-law models. For pixels on the edifice, the difference in velocity produced by the linear and ERA-Interim corrections is between 5 and 6 mm/yr. Comparing the linear and ERA-Interim corrections for individual interferograms in phase-elevation space, it can be seen that the two models predict phase delays with opposite sense of direction for some interferograms, especially at high elevations (Figure 7), causing the large discrepancy in average LOS velocities on the edifice.

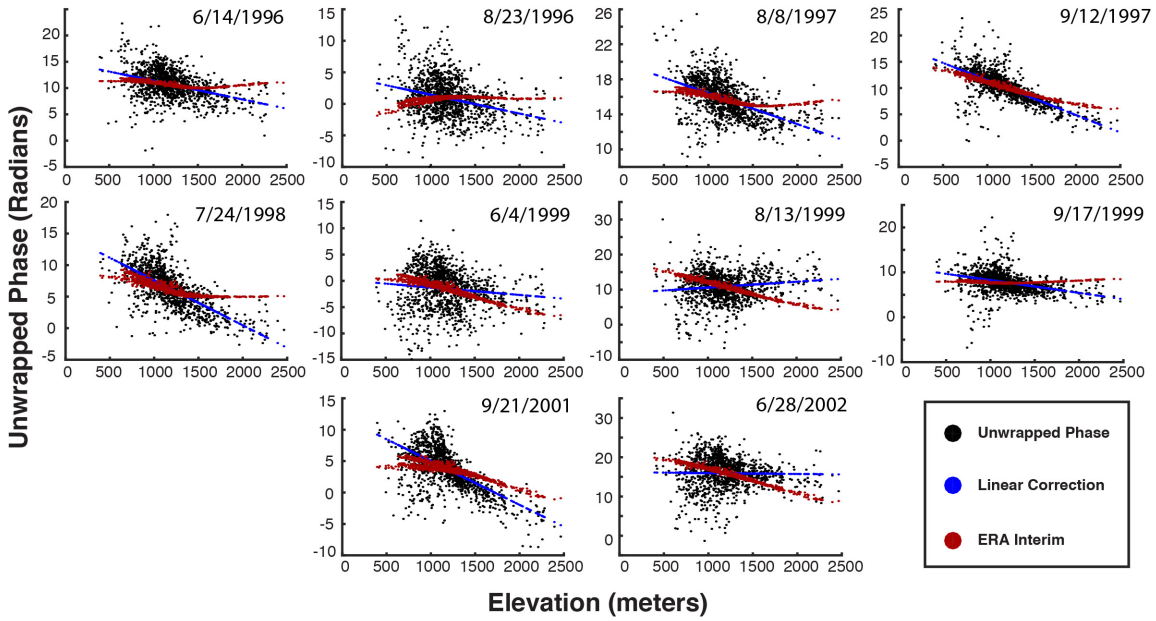

Figure 7. A comparison of the ERA-Interim (red) and basic linear (blue) atmospheric corrections for all 10 interferograms of ERS-2 track 156 in phase-elevation space. The date of the slave scene is in the upper right of each

frame. A correlation between phase and elevation is seen in the unwrapped phase of many, but not all interferograms. The two corrections predict phase delays with opposite sense of direction for some interferograms, especially at high elevations. For clarity, the number of points is reduced by a factor of 10.

5. Discussion

5.1 Atmospheric Corrections

Because the phase is correlated with topography in the vast majority of interferograms for Mount St. Helens, it is clear that an attempt should be made to model and remove atmospheric phase delay to improve the signal-to-noise. Within the category of phase-elevation based corrections, the choice between techniques does not significantly affect average velocities, as seen in Table 2. A comparison of phase based corrections produced for a single interferogram (Figure 8) shows that, except for windowed moving average corrections, the phase-based techniques are nearly indistinguishable. Methods that rely on climate reanalysis models and those that rely on the phase-elevation correlation produce similar corrections for individual interferograms in some cases. The similarities and differences between the two techniques are shown in Figure 7, which compares the linear phase-based and ERA-Interim corrections in phase-elevation space for all interferograms in a single data set. The two techniques likely agree more closely when the atmospheric conditions change more slowly and avoid being aliased by ERA-Interim temporal sampling rates. The two methods are more similar at low elevations (below 1500 meters), but tend to diverge at high elevations.

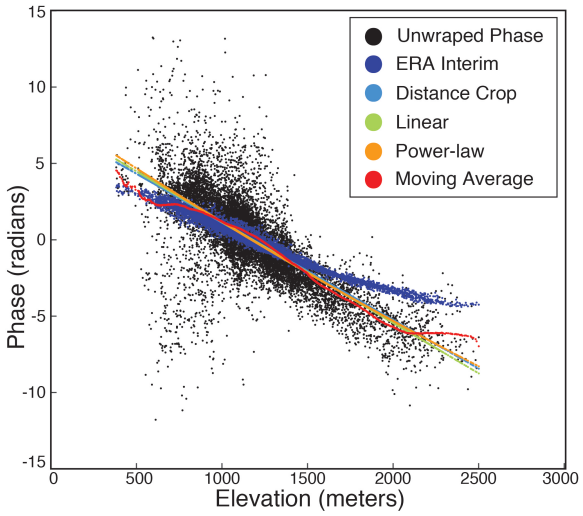

Figure 8. A comparison of atmospheric correction models for a single interferogram (ERS-2 track 156, 9/12/1997 – 8/28/1998) in phase-elevation space. A clear correlation between phase and elevation is seen in the unwrapped phase. Except for the windowed moving average, trend fitting corrections are nearly indistinguishable. The ERA-Interim model produces a similar correction to the phase based corrections, but diverges especially at high elevations.

For some interferograms, the ERA-Interim and phase-based corrections can differ greatly, which can lead to markedly different average velocities and time-series results. For example, with regard to the pre-eruptive data set from ERS-2 track 156, the two corrections produce velocities for the edifice which differ by 5-6 mm/yr on average (Figure 9). The high difference in velocities produced by the two corrections for both this ERS-2 data set and also for ENVISAT Track 20 is large enough to change the sense of direction (uplift versus subsidence) of displacements on the edifice. This implies that the choice of atmospheric correction is extremely important and has an enormous impact on studies of volcanoes with large topographically correlated atmospheric signals and low signal-to-noise.

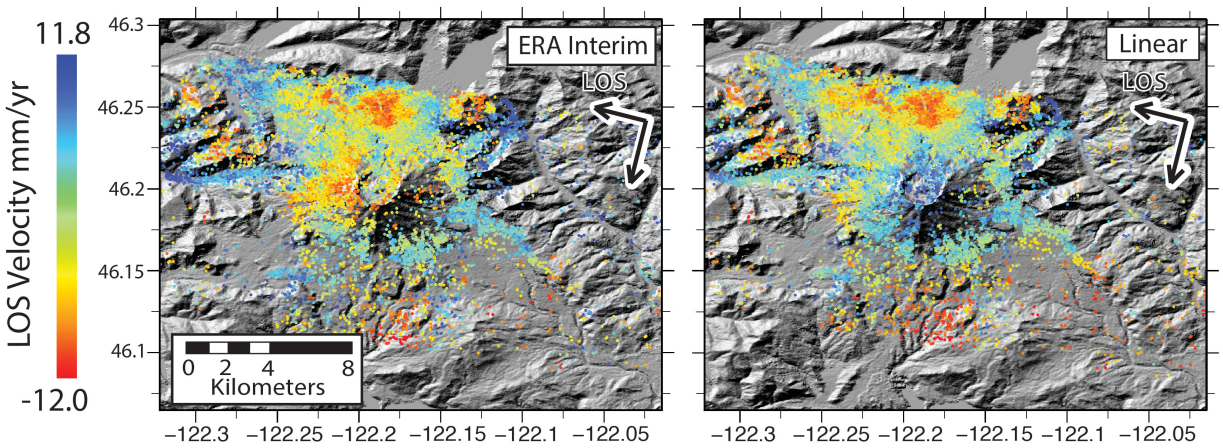

Figure 9. Comparison of average velocities produced using the ERA-Interim and simple linear corrections for ERS-2 track 156. Velocity differences on the edifice are 5-6 mm/yr on average but can exceed 10 mm/yr at some points, large enough to cause a change from apparent subsidence to uplift.

Fine scale, turbulent structures in the atmosphere produce phase delay in interferograms that cannot be represented accurately by reanalysis style corrections because of the low temporal and spatial resolution of the climate models. The residual atmospheric delay in individual interferograms that is not removed by correction techniques will affect the scatter in displacement time-series and correspondingly add uncertainty to estimates of average velocities. However, as described by Parker and others (2015), because the turbulent component of atmospheric delay does not correlate with time, averaging across at least 8 interferograms in a StaMPS data set should minimize its effect, which is manifested as a residual error in the corrected interferograms.

While phase based corrections are fast and easy to apply, and do not require the acquisition of additional data, they run the risk of removing or significantly reducing a deformation signal which is centered over a volcanic edifice. This effect is evaluated by generating synthetic interferograms with a hypothetical inflation source at Mount St. Helens that produces velocities on the edifice of 12-15 mm/yr (Figure 10). Atmospheric phase delay from one of the ERS-2 data sets, modeled by the ERA-Interim technique, is added to ten

interferograms and then the interferograms are corrected with a linear fit to phase and elevation. The resulting velocities for the edifice and crater differ from the true deformation signal by up to 12 mm/yr (Figure 10), thereby minimizing the observed uplift. Therefore, we do not expect average velocities corrected by phase and elevation trends to accurately reflect volcanic deformation in applications where the signal-to-noise or deformation rates are low. This problem is most relevant to volcanic studies, because the deformation pattern tends to be radially symmetric around the volcanic edifice. While the ERA-Interim correction cannot in theory fully remove the atmospheric signal, it does not misidentify, model, and remove volcanic deformation as atmospheric phase delay. Consequently, the ERA-Interim climate reanalysis correction method was preferred in this work, despite its drawbacks.

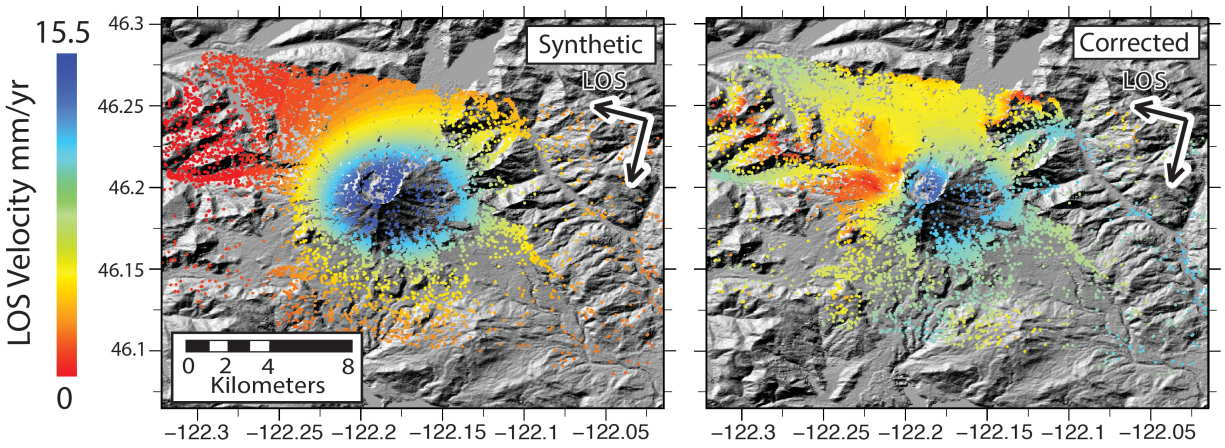

Figure 10. (Left) Synthetic average velocities produced by a spheroid model centered under the edifice with a depth of 2 km and a pressure change of 1250 MPa. The synthetic data set includes 10 interferograms using an ERS-2 viewing geometry. (Right) Velocities produced after adding synthetic atmosphere from ERA-Interim and correcting with a linear fit to phase and elevation. Velocities on the edifice differ greatly (5-10 mm/yr) from the velocities expected from deformation, indicating the shortcomings of the most simplistic phase trend fitting corrections.

5.2 Volcanic Deformation

5.2.1 PS InSAR Interpretations

Persistent Scatterer analyses of data sets covering both the pre- and post-eruptive periods of Mount St. Helens' 2004 eruption indicate that any volcanic deformation that may have occurred must have been very subtle. After correcting for atmospheric phase delay using the ERA-Interim model, maps of average velocities and time series from both of the pre-eruptive data sets show small LOS signals centered on the edifice that have inconsistent or opposite sense of direction with respect to one another (Figures 5 and 6). This inconsistency of edifice velocities is repeated for the two data sets from the post-eruptive period. In both cases, one data set shows average movement of points on the edifice towards the satellite (inflation), while the other has movement away from the satellite (subsidence). We propose that this contradiction mainly reflects the propagation of bias from the atmospheric correction to velocities, with other sources of error quite low as a result of PS processing. It is possible that a pressure change at depth leading up to the eruption was accommodated inelastically, leading to a lack of expression at the surface. The pressure change and associated surface deformation may also have occurred primarily in the final year or months leading up to the eruption and is therefore not captured by the data used in this study. One final alternative is that the surface displacements were localized to the crater where environmental factors lead to poor coherence and low density of pixels, preventing accurate observations from being made.

While the StaMPS processing was able to identify a good density of scatterers on the lower to mid edifice, not many statistically stable pixels were selected within the crater (Figure 5). Furthermore, the velocities of pixels within the crater are not as spatially coherent as those in regions of higher pixel density. Considering the low density of pixels and great variety of physical processes capable of producing surface displacements within the crater (i.e. glacial movement or erosive instability of the crater walls and lava domes), no confident interpretation can be made for that region. As was the case for the edifice, average velocities for points in the

crater had opposite sense of direction depending on the data set considered. It is likely however, that if a larger signal was present, it would be detectable.

5.2.2 Spheroid Model Resolution Testing

In order to better understand the capability of the PS InSAR and GPS data sets from the pre-eruptive period to detect a potential deformation source at Mount St. Helens, we tested their ability to resolve the depths and pressure changes of synthetic deformation sources over a range of parameter combinations. Displacements for a spheroidal source were calculated at all pre-eruptive campaign and continuous GPS locations in a 12 km radius of the mountain and at all PS pixels using scripts from Battaglia et al. (2013) which are based on equations from Yang et al. (1988) and Newman et al. (2006).

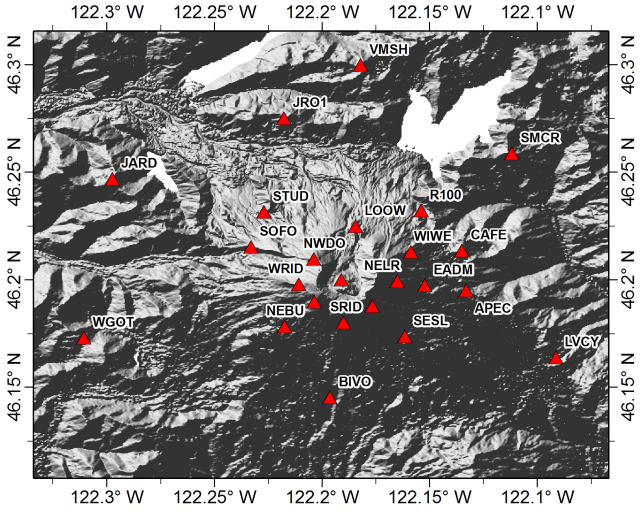

Figure 11. Locations of the 25 campaign GPS stations (Red Triangles) used in synthetic testing of spheroidal deformation sources. Stations used were within 12 km of the crater and occupied in multiple surveys prior to the 2004 eruption.

The magma chamber was assigned a long-axis radius of 500 meters and an aspect ratio of 0.5. Spatially correlated synthetic noise, which mimics the final velocity observations of this work, was added to the synthetic PS velocities. The random spatially correlated noise was generated

by first applying a two-dimensional Fourier transform to the final velocity results corrected by the ERA-Interim technique to obtain a power spectrum. The power spectrum was randomly permuted by small increments and then transformed back into the spatial domain resulting in noise with similar spatial characteristics to the input. Noise was also generated for the campaign GPS sites using the velocity uncertainties reported in Lisowski et al., (2008), which was then added to the forward modeled GPS velocities.

Surface velocities from a modeled spheroidal deformation source were calculated for 120 combinations of depth and pressure change. The ranges of depths to the magma chamber and changes in pressure were from 500 to 7000 meters, and 20 – 1000 MPa, respectively. For each parameter combination, the pressure change and depth of the chamber were estimated using a Monte Carlo approach, repeated for 1000 iterations of random spatially correlated noise. The Monte Carlo approach was used because of the non-linear relationship between the parameters and surface velocities. The 1000 best fitting depths and pressure changes, and their associated residuals were recorded for each spheroidal deformation source and utilized to quantitatively assess the ability of the GPS and InSAR data to resolve the model parameters as a proxy for detection.

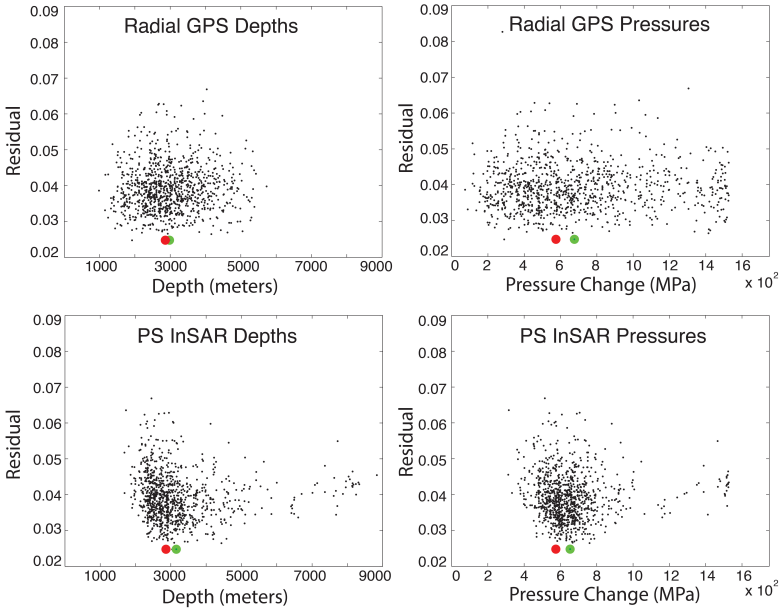

Figure 12. Monte Carlo fits of a hypothetical inflation source. Example clouds of best fitting parameter solutions for 1000 iterations of noise. The true parameter value and mean best fitting value are indicated by the red and green dots respectively. The true depth and pressure change for this example are 2860m and 575 MPa, respectively. It can be seen by comparing the widths of the clouds that PS InSAR outperforms radial campaign GPS for constraining pressure and to a lesser extent depth.

The results of the inverse modeling of synthetic velocities from a range of spheroidal deformation sources indicate that PS InSAR and the existing GPS are able to constrain both depth and pressure quite well for models with shallow depths and larger changes in pressure. Figure 12 shows the best fitting depths and pressures for an example spheroidal source with a depth of 2860 and a pressure change of 575 MPa solved over 1000 iterations of noise. The uncertainty in resolving depth or pressure for a given model, considering expected levels of noise, is represented by the standard deviation (width of the cloud) of the 1000 best fitting solutions. Figure 13 shows contours of the standard deviation of the clouds of best fitting depths and pressures over the range of all tested source parameter combinations. The standard deviations are normalized by the true value of the parameter to show the uncertainty as a percent error. The depth and pressure of models residing in areas above and to the left of the contour lines (shallow depths and high pressure change) are well resolved, and are unlikely to have occurred and remained unobserved. Models laying in the model space below the contours are poorly resolved and may have occurred in the pre-eruptive period, but remained obscured by atmospheric and other sources of noise. The results in Figure 13 B show that the PS InSAR and horizontal campaign GPS perform similarly with regards to constraining the depth of magma chambers. Interestingly, Figure 13 A reveals that PS InSAR is more capable of constraining the pressure change of the modeled deformation source in almost all cases. Additionally, as one would expect given typical GPS uncertainties, the horizontal component is far more valuable than the vertical component for resolving the model parameters.

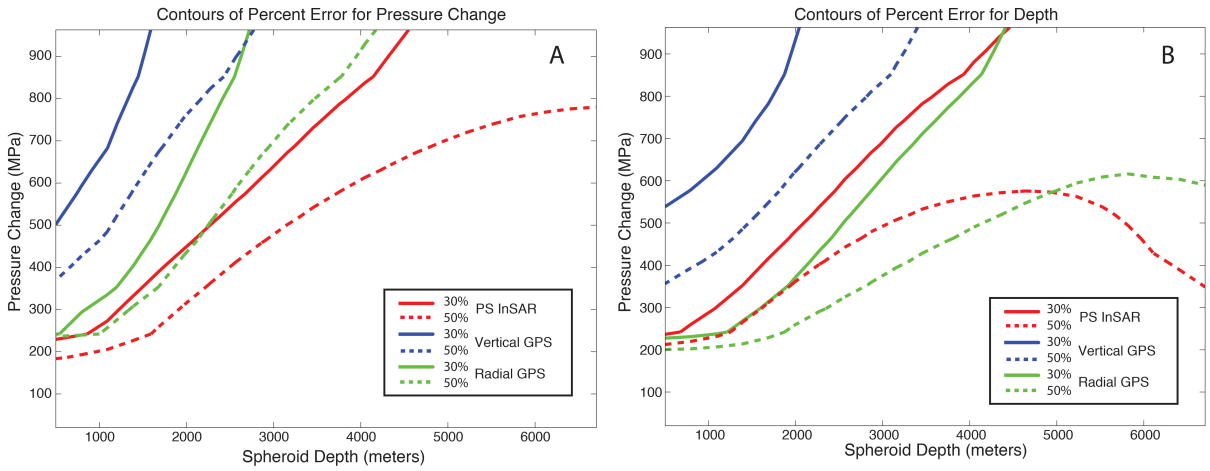

Figure 13. Model resolvability for InSAR and campaign GPS for the pre-eruptive period. Shown are contours of percent error in constraining pressure change (A) and depth (B) over the space of parameter combinations. The depth and pressure of models above and to the left of the contour lines are well resolved, and are unlikely to have occurred and remained unobserved. Models below the contours are poorly resolved and may have occurred in the pre-eruptive period, but remained obscured by noise. The 30% and 50% error contours for PS InSAR (red), vertical GPS (blue), and radial GPS (green) are represented by solid and hashed lines respectively.

Our results do not definitively rule out pre-eruptive deformation at Mount St. Helens, but they do provide improved constraints on the allowable ranges of depth and pressure change for a potential deformation source in the time period of 1996-2004. Deformation sources with combinations of pressure and depth that lie above the 30% error contour are unlikely to have occurred and remain undetected by our measurements. Models which lie outside of this contour are still within the realm of possibility of having occurred and would require some combination of larger, higher quality SAR data sets, improved interferogram coherence, and or improvements to the atmospheric data sets and correction techniques. It is assumed that deformation sources whose parameters are well resolved by the synthetic data sets are more likely to stand out from the noise and produce a confident detection in a given real data set.

Spheroidal deformation models for the co-eruptive deflation proposed by Lisowski et al. (2008) and Palano et al. (2012), derived from continuous GPS observations, suggest a source

at a depth of 7.9-8.0 km and a volume decrease of approximately 8 to 12 million cubic meters. Based on assumptions made by Palano et al. (2012), this volume change equates to a pressure change of roughly 1000 MPa. The results of the resolution test shown in Figure 13 indicate that it is likely that the authors' proposed co-eruptive deformation models would not be well resolved or detected by the SAR data used in this work.

5.3 Pumice Plain

All four data sets processed in this study consistently show definite subsidence (LOS Increase) of an area of the pumice plain ~6 km north of the edifice. The patch of subsidence covers several square kilometers and has a peak average velocity on the order of 10 mm/yr. When comparing LOS velocities between contemporaneous data sets, there are only minor discrepancies in the pre-eruptive period. Larger discrepancies on the order of 2-3 mm/yr exist between the average velocities of the two post-eruptive data sets in some locations, but they merely reflect scatter in the time series and do not suggest that the apparent subsidence is actually noise.

The subsidence signal appears more localized through time with some locations experiencing increased rates of subsidence while rates at many other locations decreased. One physical interpretation of the subsidence signal is that large amounts of ice were entrained and buried in flows during the 1980 eruption, and having being well insulated by debris are still slowly melting as suggested by Poland and Lu (2008). Another possible cause suggested by Poland and Lu is the gradual settlement and compaction of unconsolidated eruptive deposits. Finally, the subsidence can possibly be attributed to some hydrologic change in the subsurface, possibly tied to nearby Spirit Lake, which was significantly impacted by the 1980 eruption (Poland and Lu, 2008).

6. Conclusions

InSAR studies of deformation at volcanoes with high vertical relief are highly affected by atmospheric phase delays caused by changes in the distribution of water vapor through time, which must be removed in order to obtain accurate surface velocities. A statistical test on a suite of atmospheric removal techniques reveals that within the category of phase-elevation trend fitting techniques, velocity results do not vary significantly. Contrastingly, methods that use independent climate data can produce markedly different results from those corrected by a trend fitting technique. In some cases, especially when the signal-to-noise is low, the results of the two types of correction techniques differ by so much that the sense of direction of apparent ground motion is reversed. In the case of volcanic deformation centered on an edifice, methods that model atmospheric phase delay using independent climate data are preferred because, unlike the trend fitting techniques, they do not remove or reduce any real topographically correlated deformation signal.

The PS InSAR results for the two data sets covering the period of 1995 to 2002 are inconsistent with one another and do not provide conclusive evidence for any pre-eruptive deformation at a broad scale or localized to the crater or edifice. Furthermore, the velocities for the edifice and crater are quite low, on the order of 1 cm/yr or less, making any true signal difficult to distinguish from the noise. It is possible that surface deformation occurred on the edifice during the pre-eruptive period, but it was either below the level of the noise, obscured by atmospheric artifacts, or cannot be resolved with the temporal availability of data. Although subtle co-eruptive deflation of up to 15 mm/yr and a transition to post-eruptive inflation is known to have occurred through analyses of data provided by the dense GPS network installed in late 2004, the PS InSAR results again contradict one another and do not confirm the observed signal. The existence of a patch of subsidence on the pumice plain north of the edifice, discovered previously, is confirmed across all data sets from 1995 to 2010. It also appears that the subsidence slowed and has become more localized through time.

While pre-eruptive deformation is not imaged on either the edifice or in the crater, we expect that PS InSAR should successfully resolve large signals on Mount St. Helens. Resolution tests performed on synthetic spheroidal deformation data with noise analogous to that of this study are able to constrain the range of allowable depths and pressure changes of a potential source. While pre-eruptive deformation sources with low changes in pressure at greater depths are unlikely to be imaged by GPS or InSAR data available from that time period, Persistent Scatterer analyses do significantly improve the spatial density of observations and also our ability to resolve or rule out combinations of depth and pressure for a potential source.

Acknowledgements

SAR data were obtained from the WInSAR and the UNAVCO archives

This work was funded by the Geodetic Imaging program at NASA (Grant # NNX13AC15G).

References

Battaglia, Maurizio, Peter F. Cervelli, and Jessica R. Murray. "dMODELS: A MATLAB software package for modeling crustal deformation near active faults and volcanic centers." *Journal of Volcanology and Geothermal Research* 254 (2013): 1-4.

Bekaert, D. P. S., A. Hooper, and T. J. Wright. "A spatially variable power law tropospheric correction technique for InSAR data." *Journal of Geophysical Research: Solid Earth* 120, no. 2 (2015): 1345-1356.

Bekaert, D. P. S., R. J. Walters, T. J. Wright, A. J. Hooper, and D. J. Parker. "Statistical comparison of InSAR tropospheric correction techniques. "*Remote Sensing of Environment* 170 (2015): 40-47.

Beauducel, François, Pierre Briole, and Jean‐Luc Froger. "Volcano‐wide fringes in ERS synthetic aperture radar interferograms of Etna (1992–1998): Deformation or tropospheric effect?" *Journal of Geophysical Research: Solid Earth* 105, no. B7 (2000): 16391-16402.

Dee, D. P., S. M. Uppala, A. J. Simmons, Paul Berrisford, P. Poli, S. Kobayashi, U. Andrae et al. "The ERA‐Interim reanalysis: Configuration and performance of the data assimilation system." *Quarterly Journal of the royal meteorological society* 137, no. 656 (2011): 553-597.

Ding, Xiao-li, Zhi-wei Li, Jian-jun Zhu, Guang-cai Feng, and Jiang-ping Long. "Atmospheric effects on InSAR measurements and their mitigation." *Sensors* 8, no. 9 (2008): 5426-5448.

Dzurisin, Daniel. "A comprehensive approach to monitoring volcano deformation as a window on the eruption cycle." *Reviews of Geophysics* 41, no. 1 (2003).

Dzurisin, Daniel, Michael Lisowski, Michael P. Poland, David R. Sherrod, and Richard G. LaHusen. "Constraints and conundrums resulting from ground-deformation measurements made during the 2004-2005 dome-building eruption of Mount St. Helens, Washington." *US Geological Survey professional paper* 1750 (2008): 281-300.

Dzurisin, Daniel, Michael Lisowski, and Charles W. Wicks. "Continuing inflation at Three Sisters volcanic center, central Oregon Cascade Range, USA, from GPS, leveling, and InSAR observations." *Bulletin of volcanology* 71, no. 10 (2009): 1091-1110.

Emardson, T. R., M. Simons, and F. H. Webb. "Neutral atmospheric delay in interferometric synthetic aperture radar applications: Statistical description and mitigation." *Journal of Geophysical Research: Solid Earth* 108, no. B5 (2003).

Farr, Tom G., and Mike Kobrick. "Shuttle Radar Topography Mission produces a wealth of data." *Eos, Transactions American Geophysical Union* 81, no. 48 (2000): 583-585.

Foster, James, John Kealy, Tiziana Cherubini, Steven Businger, Zhong Lu, and Michael Murphy. "The utility of atmospheric analyses for the mitigation of artifacts in InSAR." Journal of Geophysical Research: Solid Earth 118, no. 2 (2013): 748-758.

Hanssen, Raymond Franciscus. *Atmospheric heterogeneities in ERS tandem SAR interferometry*. Delft University Press, 1998.

Hanssen, R. F. (2001), Remote sensing and digital image processing, in Radar Interferometry: Data Interpretation and Error Analysis, *Earth and Environmental Science*, vol. 2, pp. 200–210, edited by F. van der Meer, Kluwer Acad. Publishers, Dordrecht, Netherlands.

Homer, C.G., Dewitz, J.A., Yang, L., Jin, S., Danielson, P., Xian, G., Coulston, J., Herold, N.D., Wickham, J.D., and Megown, K., 2015, Completion of the 2011 National Land Cover Database for the conterminous United States-Representing a decade of land cover change information. *Photogrammetric Engineering and Remote Sensing*, v. 81, no. 5, p. 345-354

Hooper, Andrew, P. Segall, and Howard Zebker. "Persistent scatterer interferometric synthetic aperture radar for crustal deformation analysis, with application to Volcán Alcedo, Galápagos." *Journal of Geophysical Research: Solid Earth* 112, no. B7 (2007).

Hooper, Andrew, David Bekaert, Karsten Spaans, and Mahmut Arikan. "Recent advances in SAR interferometry time series analysis for measuring crustal deformation." *Tectonophysics* 514 (2012): 1-13.

Jolivet, Romain, Piyush Shanker Agram, Nina Y. Lin, Mark Simons, Marie-Pierre Doin, Gilles Peltzer, and Zhenhong Li. "Improving InSAR geodesy using global atmospheric models." *Journal of Geophysical Research: Solid Earth* 119, no. 3 (2014): 2324-2341.

Lisowski, Michael, Daniel Dzurisin, Roger P. Denlinger, and Eugene Y. Iwatsubo. "Analysis of GPS-measured deformation associated with the 2004-2006 dome-building eruption of Mount St. Helens, Washington." *US Geological Survey professional paper* 1750 (2008): 301-333.

Mosbrucker, A. R. "High-resolution digital elevation model of Mount St. Helens crater and upper North Fork Toutle River basin, Washington, based on an airborne lidar survey of September 2009." *US Geological Survey Data Series* 904 (2014).

Newman, Andrew V., Timothy H. Dixon, and Noel Gourmelen. "A four-dimensional viscoelastic deformation model for Long Valley Caldera, California, between 1995 and 2000." *Journal of volcanology and geothermal research* 150, no. 1 (2006): 244-269.

Palano, Mimmo, Elisa Guarrera, and Mario Mattia. "GPS ground deformation patterns at Mount St. Helens (Washington, USA) from 2004 to 2010." *Terra nova* 24, no. 2 (2012): 148-155.

Parker, Amy L., Juliet Biggs, Richard J. Walters, Susanna K. Ebmeier, Tim J. Wright, Nicholas A. Teanby, and Zhong Lu. "Systematic assessment of atmospheric uncertainties for InSAR data at volcanic arcs using large-scale atmospheric models: Application to the Cascade volcanoes, United States. "*Remote Sensing of Environment* 170 (2015): 102-114.

Poland, Michael, Roland Bürgmann, Daniel Dzurisin, Michael Lisowski, Timothy Masterlark, Susan Owen, and Jonathan Fink. "Constraints on the mechanism of long-term, steady subsidence at Medicine Lake volcano, northern California, from GPS, leveling, and InSAR." *Journal of Volcanology and Geothermal Research* 150, no. 1 (2006): 55-78.

Poland, Michael P., and Lu Zhong. "Radar Interferometry Observations of Surface Displacements during Pre-and Coeruptive Periods at Mount St. Helens, Washington, 1992-2005." US Geological Survey professional paper 1750 (2008): 361-382.

Remy, D., S. Bonvalot, P. Briole, and M. Murakami. "Accurate measurements of tropospheric effects in volcanic areas from SAR interferometry data: Application to Sakurajima volcano (Japan)." *Earth and Planetary Science Letters* 213, no. 3 (2003): 299-310.

Riddick, S. N., and D. A. Schmidt. "Time-dependent changes in volcanic inflation rate near Three Sisters, Oregon, revealed by InSAR." *Geochemistry, Geophysics, Geosystems* 12, no. 12 (2011).

Scott, William E., David R. Sherrod, and Cynthia A. Gardner. "Overview of the 2004 to 2006, and continuing, eruption of Mount St. Helens, Washington." *A volcano rekindled: the renewed eruption of Mount St. Helens* 2006 (2008): 3-22.

Simons, M., and P. A. Rosen. "Interferometric synthetic aperture radar geodesy." (2007): 391-446.

Wicks, Charles W., Daniel Dzurisin, Steven Ingebritsen, Wayne Thatcher, Zhong Lu, and Justin Iverson. "Magmatic activity beneath the quiescent Three Sisters volcanic center, central Oregon Cascade Range, USA."*Geophysical Research Letters* 29, no. 7 (2002).

Yang, Xue-Min, Paul M. Davis, and James H. Dieterich. "Deformation from inflation of a dipping finite prolate spheroid in an elastic half-space as a model for volcanic stressing." *Journal of Geophysical Research: Solid Earth* 93, no. B5 (1988): 4249-4257.

Zebker, Howard A., Paul A. Rosen, and Scott Hensley. "Atmospheric effects in interferometric synthetic aperture radar surface deformation and topographic maps." *Journal of Geophysical Research: Solid Earth* 102, no. B4 (1997): 7547-7563.

Zebker, Howard A., Falk Amelung, and Sjonni Jonsson. "Remote sensing of volcano surface and internal processes using radar interferometry." *Remote sensing of active volcanism* (2000): 179-205.